Probing the spatial dimensions of nanoscale patterns with Rutherford backscattering spectrometry

Niels Claessens(1,2), Annelies Delabie(1,3), André Vantomme(2), Wilfried Vandervorst(1,2), and Johan Meersschaut(1).*

(1) IMEC, Kapeldreef 75, BE-3001 Leuven, Belgium
(2) Quantum Solid State Physics, KU Leuven, Celestijnenlaan 200D, BE-3001 Leuven, Belgium
(3) Quantum Chemistry and Physical Chemistry, KU Leuven, Celestijnenlaan 200F, BE-3001 Leuven, Belgium
[*] Niels.Claessens@imec.be; Johan.Meersschaut@imec.be

Highlights

- The spatial dimensions of nanopatterns are quantified using RBS with a mm-sized ion beam.
- The quantification is based on the effect of the pattern on the substrate signal.
- The methodology is demonstrated for structures as small as 35 nm.

Abstract

We realize the quantitative determination of the spatial dimensions of nanopatterns using Rutherford backscattering spectrometry (RBS) with a mm-sized ion beam. The methodology is based on the effects of the nanopatterns on the RBS signal from the substrate. We demonstrate the approach with the study of a periodic pattern of 35 nm wide and 75 nm high SiO_2 lines which have a periodicity of 90 nm. We analyse the relation between the features in the experimental spectra and the properties of the nanostructures. Current voxel-based simulation software allows to reproduce many of the experimental observations well. However, we found that the present simulation software inadequately incorporates the effect of the angular spread due to the finite detector size. We propose a method to model the effect more accurately and through this we demonstrate a dramatically improved agreement with the experimental spectra.

Keywords

Ion beam analysis; Rutherford backscattering spectrometry; lateral resolution; ensemble measurements; nanostructures; nano-scale patterns; area-selective deposition

1. Introduction

Rutherford backscattering spectrometry (RBS) is a quantitative and traceable method to analyse the composition or atomic areal density in the near-surface region of a sample [1,2]. Its attractiveness relates to the quantitative description of the physical phenomena and the availability of well-established computational simulators. High spatial resolution analysis is typically pursued with highly focused analysis beams, be it at the expense of sensitivity and potential beam damage effects [3-5]. However, attempts have also been made to use RBS to characterize the shape and the size of small structures whereby the beam spot size is much larger than the feature size. Early research then focussed on interpreting the experimental spectrum of micrometre scale patterns as a superposition of blanket film spectra [5-10]. For features at the nanoscale such simplifications are no longer generally appropriate. As a partial solution, analytical expressions were derived to relate the measured spectra to the shape and the size of nanostructures for some very specific cases [11-13]. Recently, advanced software which accepts a general voxel-based description of the sample has been developed [14]. Such simulators permit to simulate the expected spectrum of arbitrary structured surfaces allowing the quantitative analysis of nanopatterned samples and have been used, amongst others, to study self-organized particles [15-17], paint [18], and periodic InGaAs nanostructures [19].

Very recently, we have reported on the analysis of the site-specific areal density in nanoscale line patterns (a periodic pattern of lines) using RBS with a mm-sized ion beam [20]. We studied the case of Ru area-selective deposition on patterns with a line width of 35 nm. The Ru growth evolution on the different areas as well as the selectivity of the deposition was quantified with a limit of detection of 10^{13} atoms/cm^2. An essential aspect of this approach is that an ensemble of identical nanostructures is measured, leading to a high count-rate due to the large volume probed, and thus excellent sensitivity and fast analysis times. Yet, detailed prior knowledge on the shape and the size of the line patterns is needed, for which we have used transmission electron microscopy (TEM).

In the present work we study the effect of the line patterns on the backscattering signal of the substrate, and we show that Rutherford backscattering can also be used to quantitatively determine the line width and the spatial periodicity of the pattern or pitch. First, we demonstrate that in the parallel measurement geometry, i.e., with the lines aligned parallel to the scattering plane, the energy loss within the lines can be used to extract information on the line width/pitch ratio of the structures. Second, we show that in the perpendicular measurement geometry, with the lines aligned perpendicular to the scattering plane, the RBS signal of the substrate shows intensity oscillations which are induced by the lateral periodicity of the line patterns. The intensity oscillations of the substrate signal can be interpreted in terms of the pitch of the structures. Hence, both key parameters of these line structures, i.e., the line width and the pitch, can be derived from the RBS analysis.

2. Materials and methods

The sample studied in this work consists of SiO_2 line patterns (figure 1) on a TiN thin film with an oxide line length of 1 cm, width of 35 nm, height of 75 nm, and a spacing of 55 nm [21]. Each patterned area on the wafer is 1 cm by 1.2 cm in size. Ruthenium area-selective chemical vapour deposition was used to grow ruthenium only on the TiN surface in between the SiO_2 lines while leaving the SiO_2 lines uncovered [21]. The studied sample corresponds to the sample shown in figure 1 and discussed in section 2 of reference [20].

TEM images were taken using methods described in the previous publication [20]. Scanning electron microscopy (SEM) images were acquired using a Hitachi 6300 operated at 2 keV. In figure 1 we show the SEM and TEM images of a SiO_2 line pattern. The dark colour in-between the SiO_2 lines reveals the presence of Ru at the bottom of the space in between the lines. We determined the width and pitch of the line patterns using these images and estimated the uncertainty by calculating the standard deviation on the measured magnitude of the width and pitch. Using top-view scanning electron microscopy we quantified the standard deviation for the line width and the pitch across the wafer as below 2 nm. The standard deviation for the height of the SiO_2 lines was derived from a TEM analysis and is less than 3 nm.

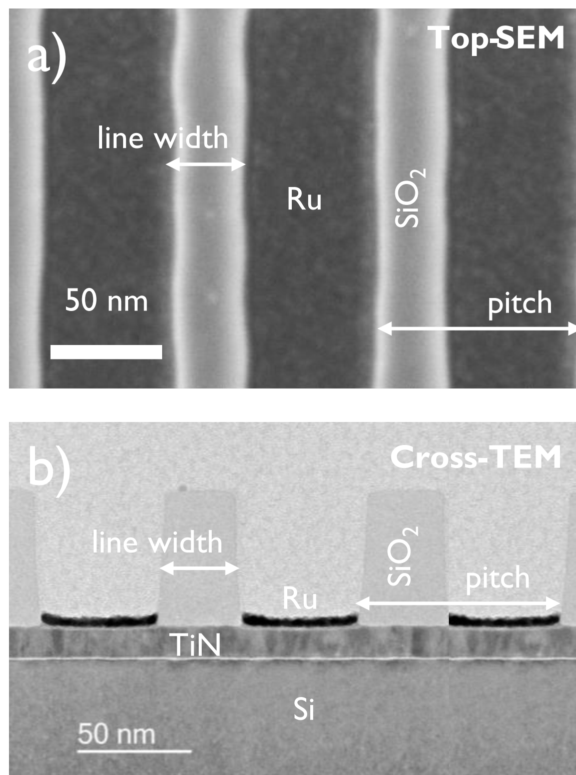

Figure 1 Top-SEM (a) and cross-sectional TEM (b) images of a SiO_2 line pattern.

The RBS experiments were conducted in a scattering chamber equipped with a sample holder mounted on a 5-axis goniometer [22]. A fixed circular detector at 135° scattering angle, and a square detector on a 360°-rotation stage were used for the experiments. The solid angle of the fixed detector is 0.42 msr whereas for the detector on the rotation stage it amounts to 1.4 msr. In some of the experiments a rectangular aperture was mounted in front of the detector on the rotation stage, thereby reducing

its acceptance angle in the scattering plane to 0.1° while keeping the angle perpendicular to this plane constant at 2.2°. The latter resulted in a solid angle of 0.07 msr. The energy resolution of the fixed detector and the movable detector is 18.7 keV and 17.5 keV, respectively. The pressure within the scattering chamber was kept well below 10^{-6} mbar during the experiment.

To perform the RBS experiments, a 1.52 MeV He^+ ion beam of 15 nA was generated with a tandem 6SDH Pelletron accelerator from National Electrostatics Corporation. Each spectrum was recorded with a total applied charge of 60 µC. The beam spot on the sample was confined to an area of 2 mm x 2 mm using slits, exposing about twenty-two thousand SiO_2 lines to the ion beam. To acquire enough counts, the RBS measurements with aperture were repeated 5 times and the spectra were added whereby each measurement was performed at adjacent but non-overlapping beam spot positions to avoid exposure effects. We made sure that during the experiments the probing beam remained well within the patterned area.

The RBS experiments were performed in two different experimental geometries. For the parallel geometry, the oxide lines were aligned parallel to the scattering plane. As shown in figure 2-a, the sample tilt was set to 30°, the fixed detector with a scattering angle of 135° was used, and the exit angle was 75°. For the perpendicular geometry, the oxide lines were aligned perpendicular to the scattering plane. As shown in figure 2-b, the sample tilt was set to 45°, the detector on the rotation stage was used and the scattering angle was set to 92°. The exit angle from the sample surface was 43°.

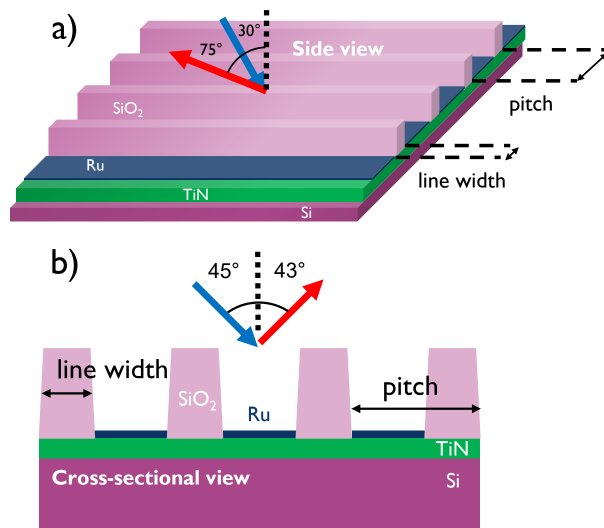

Figure 2 Schematic presentation of the ion trajectories in the parallel (a) and perpendicular (b) geometry (incoming He^+ ion: blue, outgoing He^+ ion: red).

We have followed two approaches to simulate the RBS spectra in the parallel geometry while accounting for the nanostructuring of the near surface. In the first approach the spectrum is approximated as a superposition of blanket film sub-spectra. An in-house code which automatically simulates the blanket film sub-spectra using SIMNRA and which adds them using appropriate weights was used [5, 23]. We have reported on this method in reference [5]. The drawback of this method is that not all effects due to the non-planar structure can be modelled. Therefore, to assess the impact of such effects, in the second approach we generated the spectra using a Monte-Carlo (MC) method. For each simulation a hundred thousand randomly chosen

points of incidence and backscattering on the pattern were taken, and the corresponding pathlengths within the different materials were calculated. We assumed a constant stopping power for the ingoing and outgoing path within the various materials and neglected all other contributions to the energy spread besides the detector resolution. Furthermore, we assumed constant scattering cross-sections. We will refer to this code as the *MC code*.

To simulate spectra which are acquired in the perpendicular geometry, we have used STRUCTNRA [24]. The STRUCTNRA software generates RBS spectra on patterned samples by simulating multiple pseudo-random beam incidences over a voxelated representation of the sample and using periodic boundary conditions. The procedure to construct the voxelated sample model is reported elsewhere [20]. For each trajectory, the sequence of traversed materials and pathlengths are calculated based on the intersection with the various voxels. STRUCTNRA then uses SIMNRA to calculate the corresponding sub-spectrum for each trajectory using an equivalent blanket layered sample model which are finally added. For a more detailed description of STRUCTNRA we refer the reader to reference [24]. In a few selected cases we complemented the STRUCTNRA-based analysis with MC simulations as described in the previous paragraph.

3. Results and discussion

3.1 Parallel geometry

In figure 3 we show the RBS spectrum in the parallel geometry. One notices that the titanium signal from the underlying TiN layer appears as a double peak in the spectrum. This may be qualitatively understood as follows. The trajectories for backscattering ions for two exemplary points of incidence, one on the oxide line and one on the ruthenium in between the lines, are illustrated in the schematic representation of figure 3. The energy loss for the helium ions when penetrating through the thick SiO_2 lines is much larger than for the ones penetrating through the thin ruthenium layer, which leads to the double peak for Ti in the spectrum.

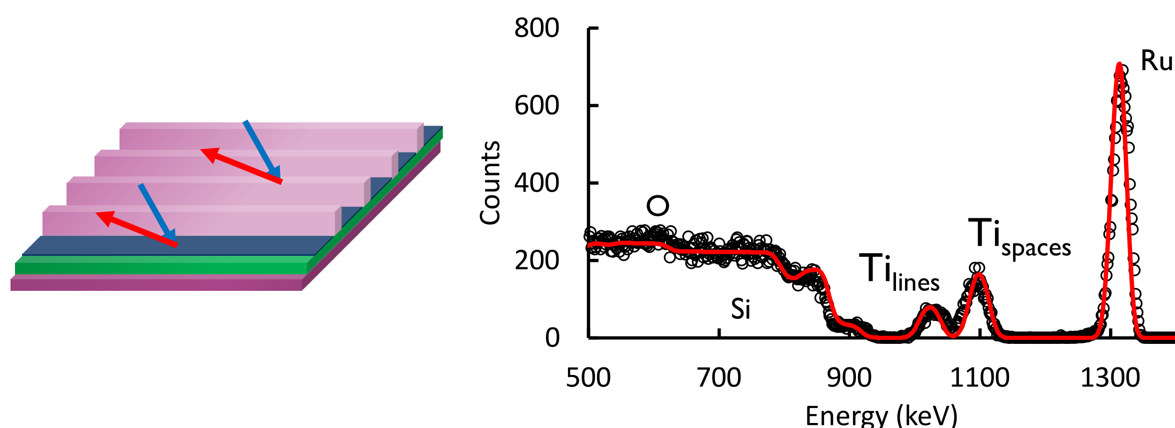

Figure 3 Experimental RBS spectrum (dots) of a SiO_2 line pattern in the parallel geometry and simulation using the approximation described in the text. The signals of Ti originating from underneath the lines and the spaces between the lines are labelled individually.

The spectra can also be quantitatively interpreted. The energy difference between the Ti peaks can be used to determine the thickness or height of the SiO_2 lines. The

integral of the titanium signal at low energy scales with the areal density of the part of the TiN layer which is covered by the oxide. Thus, with N_{lines} indicating the areal density corresponding to the low-energy Ti signal and N_{spaces} indicating the high-energy titanium signal – the coverage is:

$$\frac{width}{pitch} = \frac{N_{lines}}{N_{lines} + N_{spaces}}. \quad (1)$$

To extract the areal densities, we fit the data. Due to the symmetry of the sample in the scattering plane, it is possible to approximate the spectrum as a superposition of two blanket film sub-spectra. These blanket films represent the oxide lines (SiO_2/TiN/Si) and the space in between the lines (Ru/TiN/Si). The fit is realized with the code which automatically simulates and sums up the blanket sub-spectra as is described in the *Materials and methods* section. In the current case, the weight for the sub-spectrum representing the oxide lines is the width/pitch ratio, while the weight for the other sub-spectrum is one minus this ratio. During the fitting, the width/pitch ratio was treated as a fitting parameter. This leads to the fit shown in figure 3 and to the corresponding value for the width/pitch ratio of 0.36 (0.02), agreeing very well with the value of 0.36 (0.02) obtained from TEM. The latter ratio was estimated from the average width and pitch of the pattern observed in the transmission electron microscopy images (figure 1) for which the uncertainty is dominated by the variation of the width observed for different lines. As can be seen in figure 3, although the simulation does reproduce the Ti double peak, the experimental signals for Ti are broadened in-between the peaks as compared to the simulation. We address the origin of this effect below.

The above approach assumes a perfect parallel alignment of the scattering plane to the lines, and the detection with a point-like detector. The angular spread perpendicular to the scattering plane which is captured by the finite-sized detector is illustrated in figure 4-a, while the effect of a potential misalignment is shown in figure 4-b. Both these effects lead to ions entering/exiting the oxide lines from the sidewalls, which is not covered by the simulation as this is an effect of the non-planar sample structure. Additionally, the fitting of the spectrum with two discrete contributions, as it is presented above, would reflect the presence of perfectly square SiO_2 lines on top of the TiN layer whereas, in reality, the lines have a tapered shape as is illustrated in figure 4-c. The inclination of the edges has a similar effect on the ion trajectories as the angular spread: i.e., ions entering/exiting the oxide lines from the sidewalls. The varying energy loss in these cases could cause the broadening of the leading edge of the Ti signal at low energy and the broadening of the trailing edge of the Ti signal at high energy.

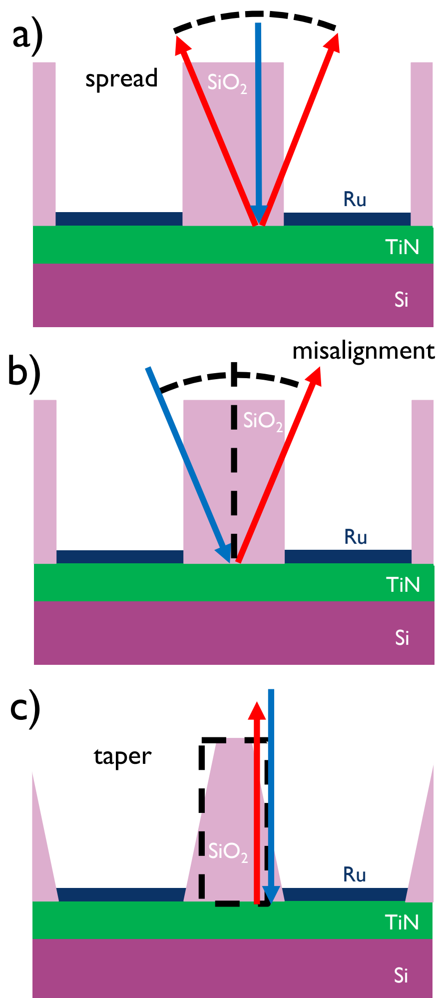

Figure 4 Illustration of (a) the angular spread, (b) the potential misalignment, and (c) the tapered shape of the SiO_2 in the parallel geometry (incoming He^+ ion: blue, outgoing He^+ ion: red). Note that the effects are grossly exaggerated for illustration purposes.

We estimated the impact of the angular spreading, a possible misalignment (up to 1°) and the tapered shape of the lines on the experimental spectrum by taking them into account in the simulation of the expected spectrum using the *MC code* described in the *Materials and methods* section. The resulting spectrum was scaled to the experimental data and plotted in figure 5 together with the experimental spectrum and the initial simulation from figure 3. It is apparent that the experimental data are modeled better when the above effects are included. The uncertainty from the effects listed above to the quantification of the width/pitch ratio was estimated by repeating the analysis on the spectra generated by the *MC code* and comparing to the input values of the simulations. For the present case the uncertainty is estimated as 3%. The relative uncertainty is, however, line-size dependent: a higher relative uncertainty is expected for finer lines.

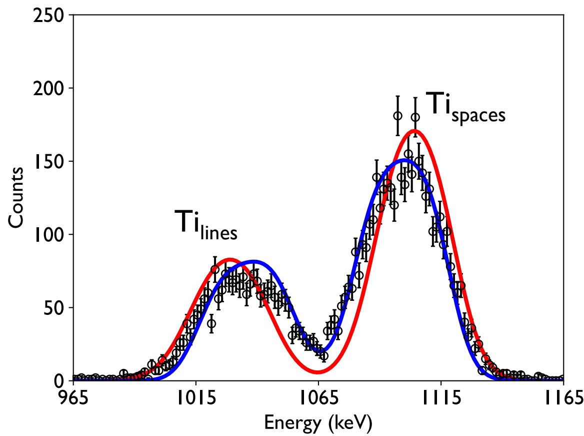

Figure 5 Zoom-in on the experimental RBS spectrum (dots) of a TiN layer covered with a SiO_2 line pattern in the parallel geometry. A simulation using a superposition of blanket film spectra (red line) and a simulation using the Monte-Carlo method discussed in the text (blue line) are shown. The signals of Ti originating from underneath the lines and the spaces between the lines are labelled individually.

3.2 Perpendicular geometry

In figure 6 we show the Rutherford backscattering spectrum obtained in the perpendicular scattering geometry and with the rectangular aperture in front of the detector. In the figure, we also plot the simulation of the spectrum using STRUCTNRA. The simulation agrees well with the experimental data obtained on the SiO_2 line pattern. The signal for backscattering from Si in the SiO_2 lines can be found at 1120 keV, while the signal for backscattering from Si in the substrate is found below 1100 keV. Most strikingly, the substrate signal contains intensity oscillations as a function of energy. We recognized that the experimental observations are reminiscent of effects reported in the theoretical studies in references [25-26]. We will address the origin of the intensity oscillations below.

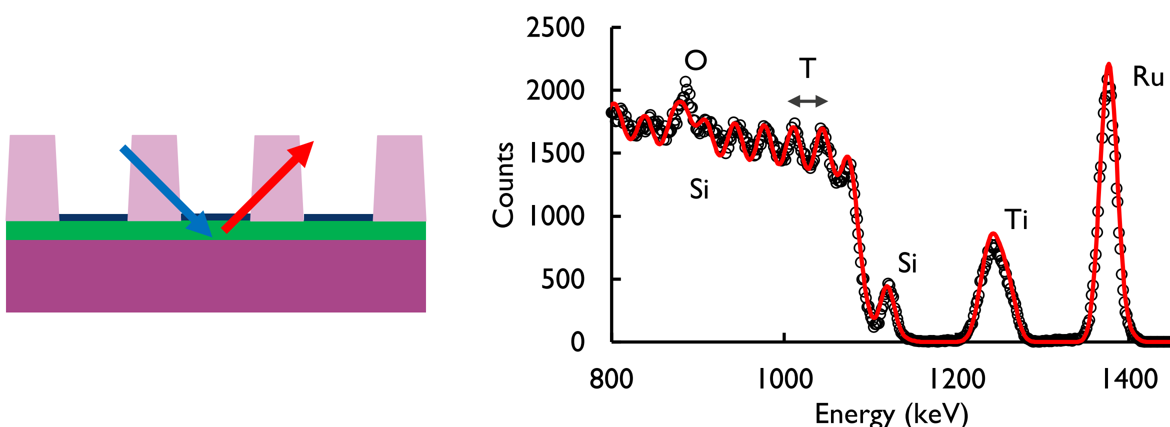

Figure 6 The experimental RBS spectrum (dots) of a SiO_2 line pattern in the perpendicular geometry and simulation using STRUCTNRA.

We organize the discussion as follows. First, we consider a freely chosen point of incidence on the pattern. We will show that the contribution of this point of incidence to the Si substrate signal features oscillations as a function of energy for which the

period can be related to the pitch. Second, we will show that the theoretical RBS spectrum which is the superposition of all contributions for varying points of incidence features oscillations with the same periodicity. Third, we will show that the amplitude of the oscillations does not go to zero.

The trajectories for backscattering ions for one exemplary point of incidence on the pattern are illustrated in figure 7-a. Like in the case of the parallel geometry, the energy loss for the backscattered ions when exiting through the thick SiO_2 lines is much larger than for those exiting through the thin ruthenium layer. This causes part of the substrate signal to be shifted to a lower energy leading to a dip and an enhancement of the intensity. In figure 7-b we have drawn the backscattering trajectories within the substrate for the same point of incidence and for which the energy loss in the lines is maximum. It is observed that the phenomenon occurs repeatedly with increasing depth due to the periodicity of the sample. Thereby, note that the increment of the path length for the consecutive trajectories each time is the same. The increment is equal to the sections indicated in black in figure 7-b. Thus, given a slowly varying stopping power in the substrate, the surface structure induces a periodic intensity modulation of the substrate signal. We calculate the path length difference and thus estimate the corresponding energy loss by using the triangle identities. For a given incidence angle (α), exit angle (β), and with S and K the stopping power and kinematic factor in the substrate, the period of the oscillations (T) is related to the pitch:

$$T = S \cdot pitch \cdot \frac{(K\cos(\alpha) + \cos(\beta))/(\cos(\alpha)\cos(\beta))}{\tan(\alpha) + \tan(\beta)}. \quad (2)$$

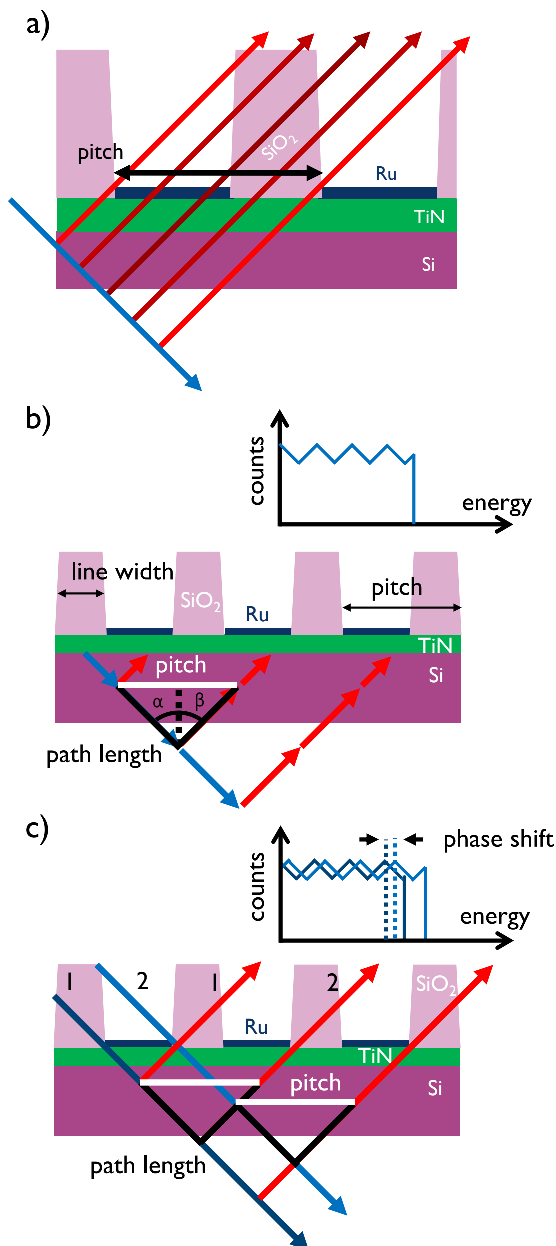

Figure 7 Schematic of the ion trajectories in the perpendicular geometry (incoming He ion: blue, outgoing He ion: red). (a) The energy loss due to the non-planar sample structure causes part of the substrate signal to be shifted to lower energies. (b) The sample periodicity causes the contribution of the substrate signal for a random point of incidence to feature oscillations which can be related to the pitch. (c) For any point of incidence, the period of the oscillations is the same while the phase can differ.

So far, we have considered only one point of incidence. Naturally, the RBS spectrum contains many backscattering events with differing points of incidence. In figure 7-c we have drawn the backscattering trajectories of maximum energy loss in the lines for two different points of incidence. One sees that the argument in the above paragraph can be repeated such that the period of the oscillations is identical and follows equation (2) irrespective of the point of incidence. On the other hand, the oscillations from the two contributions are now phase shifted with respect to each other. We have sketched the expected contribution to the Si part of the spectrum for the two points of incidence in figure 7-c. We build on the fact that the superposition of periodic signals with the

same period results in oscillations with the same periodicity. However, the amplitude of the oscillations could go to zero due to destructive interference, which depends on the phase shifts.

The phase shift between the oscillations of any two points of incidence can be estimated from the energy difference of the first minimum of the oscillations. For example, for the two points of incidence in figure 7-c this corresponds to the energy loss difference of the trajectories numbered by 1 and 2 in the figure. One sees that, a larger path within the oxide corresponds to a smaller path within the Si substrate. This has the effect of lowering the phase difference of the two contributions. More generally, we estimated the impact of the effect on the phase shifts for many different points of incidence by performing a simulation using the *MC code* described in the *Materials and methods* section. We found that the phase shift distribution is sharply peaked with more than half of the contributions having a phase shift within $\pi/5$ radians of each other. This causes the amplitude of the oscillations in the spectrum to be substantial. Note that we intentionally have chosen an experimental geometry to maximize the amplitude of the oscillations.

The pitch for the SiO_2 line pattern obtained from the RBS analysis following equation (2) is 95 (8) nm. The error is dominated by the uncertainty on the period of the oscillations which is estimated by determining the energies of the minima and maxima of intensity. The value obtained with RBS agrees with the value of 89.8 (1.2) nm which is obtained with TEM.

In the following we discuss the effect of the angular spread on the oscillations of the substrate signal in the perpendicular geometry. Indeed, it is known to the community that angular spread introduces an apparent energy spread, due to the difference in the path lengths of the particles in the various sub-layers and their related energy loss [27,28]. A computational model for the angular spread is implemented in SIMNRA, hence it is also available in STRUCTNRA [23,24].

In figure 8-a, we reproduce the experimental Si substrate signal from figure 6 with the aperture in front of the detector, while in figure 8-b we show the signal obtained from the same sample without the aperture. For both cases, the angular spread is illustrated in the figure insets. The blue lines show the simulations obtained with STRUCTNRA. One notices that the experimental intensity oscillations are more pronounced in figure 8-a as compared to figure 8-b. Whereas the STRUCTNRA simulations reproduce the experimental data well when the acceptance angle within the scattering plane is small (figure 8-a, 0.1°) they overestimate the oscillations when the angle becomes large (figure 8-b, 2.2°). This discrepancy hints towards an additional effect of the large acceptance angle of the detector in the scattering plane, which is not included in the existing simulation software. We will discuss the origin of the discrepancy below.

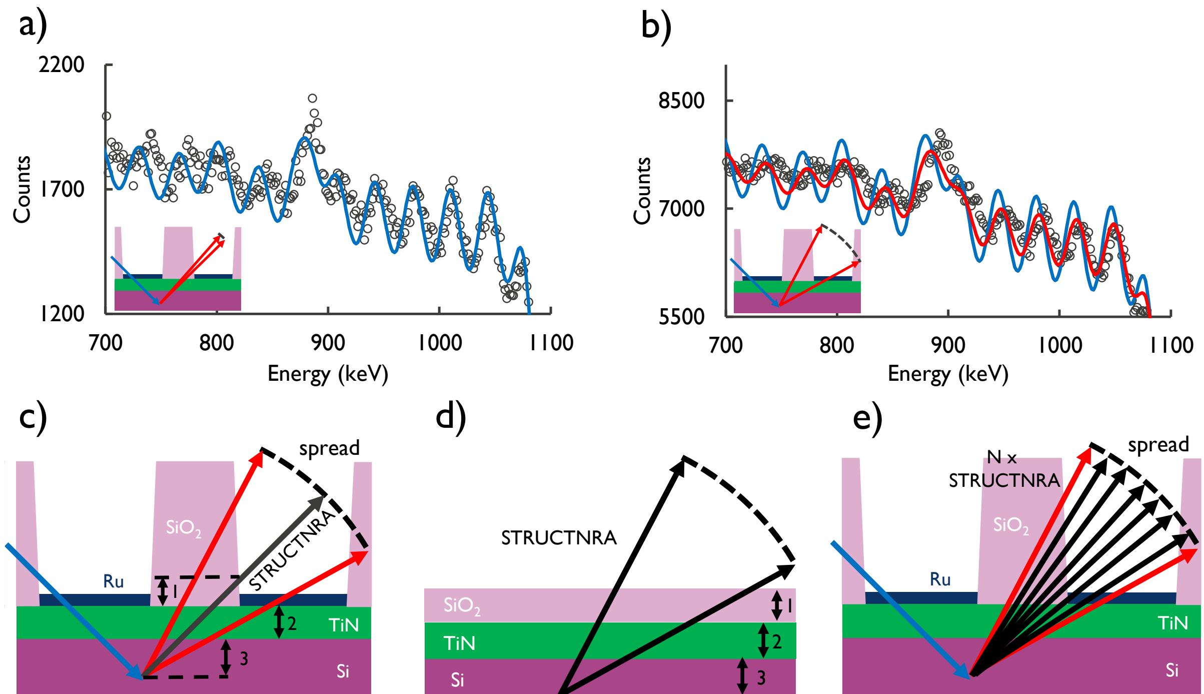

Figure 8 Zoom-in on the experimental Rutherford backscattering spectrum (dots) of a SiO_2 line pattern on a Si substrate in the perpendicular geometry (a) with, (b) without the aperture in front of the detector. A simulation using STRUCTNRA (blue line) and simulation using the method discussed in the text (red line) are shown. (c) Schematic of the angular spread on the ion trajectories in the perpendicular geometry (incoming He^+ ion: blue, outgoing He^+ ion: red, path used by STRUCTNRA: black). (d) Model of the equivalent blanket layered sample for the outgoing trajectory in (c) and treatment of the angular spread on the ion trajectory within STRUCTNRA. (e) Schematic of the procedure to incorporate the angular spread in the simulations as discussed in the main text. Note that the angular spreading in the schematics are grossly exaggerated for illustration purposes.

In figure 8-c we illustrate the angular spread on the exit angle, which in the current case is primarily caused by the large acceptance angle of the detector in the scattering plane. It is clear from the schematic that trajectories ending on the detector could have experienced different energy losses since they might traverse different materials and films. At present, STRUCTNRA calculates the expected spectrum by assuming that all exiting trajectories experience the same stack as represented by the trajectory ending up in the center of the detector (cfr. the black arrow in figure 8-c). It uses SIMNRA to calculate the corresponding sub-spectrum for each trajectory using an equivalent blanket layered sample model and models the angular spread as illustrated in figure 8-d. Hence the effect of the angular spread is handled in the equivalent blanket film model (figure 8-d) rather than in the voxel representation of the patterned sample (figure 8-c). Clearly, the energy loss difference of the exiting trajectories in the patterned sample are not captured by the equivalent blanket film model. We investigated whether this could have led to the observed overestimation of the oscillations by an underestimation of the energy spread.

For this, we performed several STRUCTNRA simulations with different exit angles which are chosen equally distributed over the exit angles to cover the angular spread of the detector, and we averaged over the resulting simulations. The approach is illustrated in figure 8-e: the black arrows represent the path of the exiting ions within the different simulations and illustrate that different backscattered particles traverse

different amounts of material. The individual simulations are performed with STRUCTNRA assuming a point detector and an equal weight is used to average them. This is justified since the detector is rectangular and aligned with the scattering plane [27,28]. The result of this procedure is shown as the red line in figure 8-b, and it fits the experimental data much better. Therefore, we have demonstrated that it makes a significant difference if the angular spread on the (exit) angle is treated within the voxel representation of the patterned sample instead of in the underlying blanket layer simulations.

4. Conclusion

We studied the effects of nanopatterns on the Rutherford backscattering spectrometry spectrum of the substrate. We have demonstrated the sensitivity of Rutherford backscattering spectrometry to the line width and the pitch of SiO_2 line patterns. From RBS spectra obtained in the parallel scattering geometry, the line width/pitch ratio of the structures can be deduced, while the pitch of the nanostructures can be derived from the RBS spectra obtained in the perpendicular scattering geometry. We also proposed to model the angular spread of the detected ions by averaging over multiple simulated spectra for which the angles are varied in the voxel representation of the sample.

Acknowledgements

We thank Masoud Dialameh, Quan Bai, and Paul van der Heide (imec) for useful discussions. We thank Johan Desmet, Praveen Dara, and Michiel Jordens (imec) for help with the experiments and simulations. We thank Olivier Richard (imec) for the transmission electron microscopy images.

Funding: This work was supported by the European Union’s Horizon 2020 research and innovation programme [grant number 824096 – RADIATE] and by the Research Foundation – Flanders (FWO) [grant number 1S45421N].

References

[1] Chu, W.-K., Mayer, J. W., Nicolet, M.-A. Backscattering Spectrometry (Academic Press, 1978).

[2] Jeynes, C., Barradas, N. P., Szilágyi, E. Accurate Determination of Quantity of Material in Thin Films by Rutherford Backscattering Spectrometry. *Anal. Chem.* **84**, 6061-6069 (2012).

[3] Ponomarev A. G., Ponomarov A. A. Beam optics in nuclear microprobe: A review. *Nucl. Instrum. Methods Phys. Res., B.* **497**, 15-23 (2021).

[4] Cookson J. A. SPECIMEN DAMAGE BY NUCLEAR MICROBEAMS AND ITS AVOIDANCE. *Nucl. Instrum. Methods Phys. Res., B.* **30** 324-330 (1988).

[5] Claessens N. *et al*. Ensemble RBS: probing the compositional profile of 3D microscale structures. *Surf. Interfaces*. **32**, 102101; 10.1016/j.surfin.2022.102101 (2022).

[6] Guo, X.S., Lanford, K.P. Rodbell, W.A. Lanford, Rodbell, K.P. A 2-dimensional RBS simulation program for studying the edges of multilayer integrated circuit components. *Nucl. Instrum. Methods Phys. Res., B.* **45**, 157-159 (1990).

[7] Berning, P.R., Niiler, A. Backscattering analysis of thin films on non-flat surfaces. *Nucl. Instrum. Methods Phys. Res., B.* **73**, 178-190 (1993).

[8] Mangelinck, D., Lee, P.S., Osipowitcz, T., Pey, K.L. Analysis of laterally non-uniform layers and sub-micron devices by Rutherford backscattering spectrometry. *Nucl. Instrum. Methods Phys. Res., B.* **215**, 495-500 (2004).

[9] Healy, M.J.F., Torres, M., Painter, J.D. A software tool enabling the analysis of small lateral features without the use of a micro-beam. *Nucl. Instrum. Methods Phys. Res., B.* **249**, 789-791 (2006).

[10] Langhuth, H., Mayer, M., Lindig, S. Layer morphology analysis of sputter-eroded silicon gratings using Rutherford backscattering. *Nucl. Instrum. Methods Phys. Res., B.* **269**, 1811-1817 (2011).

[11] Stoquert, J. P., Szörényi T. Determination of the number and size of inhomogeneities in thin films by ion beam analysis. *Phys. Rev. B.* **66**, 144108; 10.1103/PhysRevB.66.144108 (2002).

[12] Barradas, N.P. Can quantum dots be analysed with macrobeam RBS? *Nucl. Instrum. Methods Phys. Res., B.* **261**, 435-438 (2007).

[13] Barradas, N.P., Núñez, C.G., Redondo-Cubero, A., Shen, G., Kung, P., Pau, J.L. Analytical simulation of RBS spectra of nanowire samples. *Nucl. Instrum. Methods Phys. Res., B.* **371**, 116-120 (2016).

[14] Mayer, M. Malinský, P., Schiettekatte, F., Zolnai, Z. Intercomparison of ion beam analysis software for the simulation of backscattering spectra from two-dimensional structures. *Nucl. Instrum. Methods Phys. Res., B.* **385**, 65-73 (2016).

[15] Zolnai, Z., Deák, A., Nagy, N., Tóth, A.L., Kótai, E., Battistig, G. A 3D-RBS study of irradiation-induced deformation and masking properties of ordered colloidal nanoparticulate masks. *Nucl. Instrum. Methods Phys. Res., B.* **268**, 79-86 (2010).

[16] Zolnai, Z., Nagy, N., Deák, A., Battistig, G., Kótai E. Three-dimensional view of the shape, size, and atomic composition of ordered nanostructures by Rutherford backscattering spectrometry. *Phys. Rev. B.* **83**, 233302; 10.1103/PhysRevB.83.233302 (2011).

[17] Zolnai, Z. Shape, size, and atomic composition analysis of nanostructures in 3D by Rutherford backscattering spectrometry. *Appl. Surf. Sci.* **281**, 17-23 (2013).

[18] Mayer, M., Silva, T.F. Computer simulation of backscattering spectra from paint. *Nucl. Instrum. Methods Phys. Res., B.* **406**, 75-81 (2017).

[19] Laricchiuta, G., Vandervorst, W., Vickridge, I., Mayer, M., Meersschaut, J. Rutherford backscattering spectrometry analysis of InGaAs nanostructures. *J. Vac. Sci. Technol. A*. **37**, 020601; 10.1116/1.50795 (2019).

[20] N. Claessens *et al.* Quantification of area-selective deposition on nanometer-scale patterns using Rutherford backscattering spectrometry. *Sci. Rep.* **12**, 17770; 10.1038/s41598-022-22645-8 (2022).

[21] Grillo F. *et al*. Area-Selective Deposition of Ruthenium by Area-Dependent Surface Diffusion. *Chem. Mater.* **32**, 9560−9572 (2020).

[22] Meersschaut, J., Vandervorst, W. High-throughput ion beam analysis at imec. *Nucl. Instrum. Methods Phys. Res., B.* **406**, 25-29 (2017).

[23] Mayer, M. SIMNRA, a Simulation Program for the Analysis of NRA, RBS and ERDA. *Nucl. Instrum. AIP Conf. Proc*. **475**, 541-544 (1999).

[24] Mayer, M. Computer simulation of ion beam analysis of laterally inhomogeneous materials. *Nucl. Instrum. Methods Phys. Res., B*. **371**, 90-96 (2016).

[25] van Dijk, L. *et al.* Macrochannelling: Characterisation of nano-structures by ion beam analysis. *Nucl. Instrum. Methods Phys. Res., B.* **231**, 130-135 (2005).

[26] Schiettekatte, F., Chicoine, M. Spectrum simulation of rough and nanostructured targets from their 2D and 3D image by Monte Carlo methods. *Nucl. Instrum. Methods Phys. Res., B.* **371**, 106-110 (2016).

[27] Szilágyi, E., Pászti, F., Amsel, G. Theoretical approximations for depth resolution calculations in IBA methods. *Nucl. Instrum. Methods Phys. Res., B.* **100**, 103-121 (1995).

[28] Szilágyi, E. Energy spread in ion beam analysis. *Nucl. Instrum. Methods Phys. Res., B.* **116-163**, 37-47 (2000).